7-2021

Chapter 2.2: 3-D Topo Surface Visualization of Metal Ion Anti-Buffering: An Unexpected Behavior in Metal–Ligand Complexation Systems

Garon C. Smith
University of Montana, Missoula

Md Mainul Hossain
North South University, Bangladesh

Daniel D. Barry
Intel Corporation

Chapter 2.2
3-D Topo Surface Visualization of Metal Ion Anti-Buffering: An Unexpected Behavior in Metal–Ligand Complexation Systems

[1]Garon C. Smith, [2]Md Mainul Hossain and [1]Daniel D. Barry
[1]Department of Chemistry and Biochemistry, University of Montana, Missoula, MT, USA [2]Department of Biochemistry and Microbiology, North South University, Dhaka, Bangladesh

Abstract
Diluting a system that contains metal complexes can sometimes cause surprises. This chapter describes "metal ion anti-buffering", a situation in which free metal ion concentrations rapidly increase as system dilution drives dissociation. It only occurs under excess free ligand conditions when a solution is dominated by higher stoichiometry complexes. The Law of Mass Action is used to provide a mathematical justification for the phenomenon. A Cu^{2+}-ethylenediamine mixture exhibits this phenomenon when excess free ethylenediamine (en) is present. For example, it occurs when diluting a solution containing a four-fold excess of en over Cu^{2+}. As this mixture is diluted by a factor of ~5600, the modeled free Cu^{2+} concentration shows a ~470-fold increase. Taken together, this is 2.5 million times higher than dilution of the system would yield in other circumstances. Included are experimental data confirming anti-buffering in the Cu^{2+}-en system. Many other metal-ligand systems can display this behavior. Four additional examples are illustrated including an amino acid under physiological pHs. Anti-Buffering TOPOS, a downloadable Excel workbook in a supplemental file, allows readers to simulate this behavior for many metal-ligand systems. A PowerPoint lecture and teaching materials are also provided, suitable for inclusion in upper division and graduate courses in analytical chemistry, biochemistry and geochemistry.

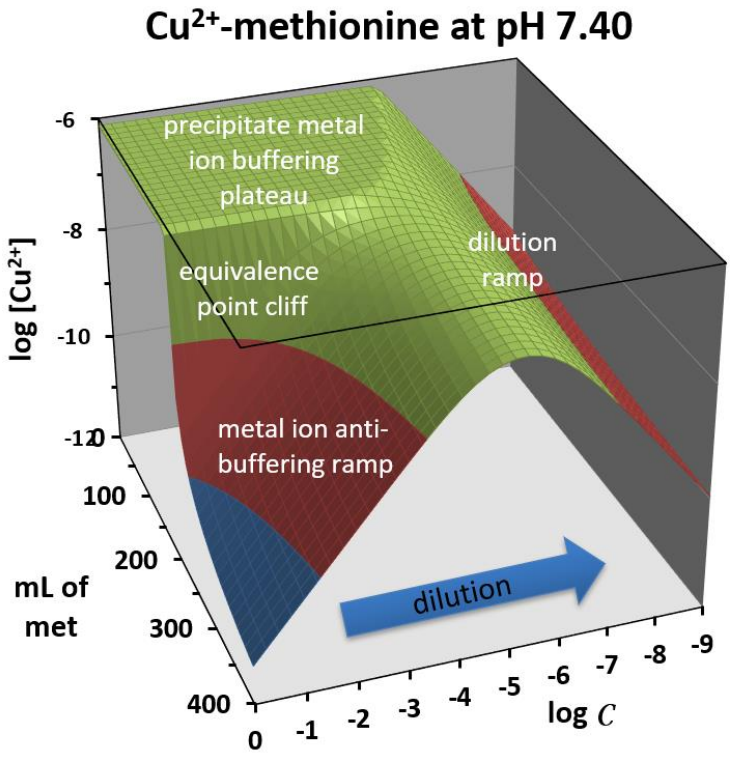

2.2.1 Introduction

Would you believe there is a situation in which an aqueous system is diluted by a factor of thousands and the concentration for one of its species is now hundreds or thousands of times greater? This can occur in many metal-ligand systems under excess free ligand conditions where higher stoichiometries of mononuclear complexes (1:2 or higher) dominate. We call this previously undescribed chemical phenomenon "metal ion anti-buffering". In this chapter, anti-buffering in a Cu^{2+}-ethylenediamine system is modeled and experimental data validating its existence are presented. The modeled system at pH 5.50, for example, shows a 469-fold increase in $[Cu^{2+}]$ as the system is diluted by a factor of 5,623. Taken together (469 x 5,623), the concentration of Cu^{2+} ion is 2.64 million times higher than dilution of the system would yield in other circumstances.

This is the second chapter that presents aqueous equilibrium behavior in metal-ligand systems as trend surfaces (topos) constructed above composition grids. The composition grid, as in all previous chapters, is a titration/dilution construct. Chapter 2.1 covered metal ion buffering as it occurs in systems that form exclusively 1:1 complexes, for example with EDTA. Metal ion anti-buffering

is simply an extension of metal ion buffering for systems where higher stoichiometries dominate. It is a manifestation of complex dissociation through the mass action effect that occurs during dilution procedures when free ligand terms in the equilibrium constant expression have exponents greater than 1. The topo trend surface approach used here makes it easy to visualize.

Aqueous systems in which a metal complex contains more than a single ligand moiety are very common, *e.g.,* copper(II) tetraamine ion, $Cu(NH_3)_4^{2+}$. Thus, they are important for students in several fields to understand. For chemistry students, most metal complexation reactions include systems with higher stoichiometries.[1-3] The copper(II)–ammonia system is routinely used in many introductory laboratories as a model system for metal–ligand reactions and a confirmation step in qualitative analysis schemes.[4] In biochemistry, metal complexation helps explain how amino acids and carboxylic acids in the Krebs cycle interact with metal ions.[5] With geochemistry, higher stoichiometry complexes are important in the fate and transport of toxic heavy metals and radionuclides in the environment.[6] Here, more than in any other setting, the conditions for metal ion anti-buffering may be encountered.

A free, down-loadable computer program, Anti-Buffering TOPOS, has been created for systems with higher mononuclear complexes. It is provided as a supplemental file in this chapter. Anti-Buffering TOPOS can create 3-D trend surfaces above a composition grid that encompasses a wide range of solution conditions. The composition grid used here is "mL of ligand" as the x-axis and the system concentration, "log C", for the y-axis. Here, C represents the molarity (mol/L) of both the metal ion and ligand solutions before a titration begins. It assumes that 100 mL of the metal ion solution are being titrated with an equimolar concentration of ligand. Thus, equivalence points will come at 100-mL increments. Log C progresses through nine orders of magnitude in concentration, from 1 M to 10^{-9} M. Variables plotted on the z-axis include log free metal (log $[M^{n+}]$), log free ligand (log [L]), concentrations of various stoichiometries of metal-ligand complexes (log $[ML_n]$), protonated ligand forms (log $[H_nL]$, hydroxy-metal complexes (log $[M(OH)_n]$), and species distribution coefficients (α's and γ's). Use of this program is appropriate for students in advanced chemistry and applied chemistry courses, namely, junior-level analytical chemistry, instrumental analysis, biochemistry and aqueous geochemistry.

2.2.2 A Mathematical Justification for Metal Ion Anti-Buffering

Consider a theoretical examination of a simplistic system where a 1:n complex dominates. The treatment below employs an overall stability constant, β_n. An overall constant cumulates individual stepwise formation constants, *e.g.,* $\beta_3 = \mathcal{K}_{F1} \times \mathcal{K}_{F2} \times \mathcal{K}_{F3}$. In eq 2.2-1, M represents the uncomplexed metal ion and L the free ligand.

$$M + n\,L \rightleftharpoons ML_n \qquad (2.2\text{-}1)$$

Charges on species and coordinated water molecules have been omitted in this treatment to keep the mathematics less cluttered.

Under excess free ligand conditions, while the maximum degree of anti-buffering is occurring, the major species in the solution will be the dominant complex, ML_n, and excess free ligand, L. Only a trace amount of the free metal ion, M, is present. If the solution is diluted by a factor of f_{dil} at constant pH, the concentrations of both major species, $[ML_n]$ and [L], will essentially drop by the same $1/f_{dil}$ factor. But, no matter what the degree of dilution, the value of β_n is a constant. Thus, the equilibrium constant expression for β_n can be written in both a "before" dilution and an "after" dilution state.

$$\beta_n = \frac{[ML_n]}{[M]_{before}[L]^n} \approx \frac{\frac{[ML_n]}{f_{dil}}}{[M]_{after}\left(\frac{[L]}{f_{dil}}\right)^n} \qquad (2.2\text{-}2)$$

Rewriting these relationships in terms of the free metal concentrations for the before dilution and after dilution states yields:

$$[\mathrm{M}]_{\text{before}} = \frac{[\mathrm{ML}_n]}{\beta_n [\mathrm{L}]^n} \quad \text{and} \quad [\mathrm{M}]_{\text{after}} \approx \frac{\frac{[\mathrm{ML}_n]}{f_{\text{dil}}}}{\beta_n \left(\frac{[\mathrm{L}]}{f_{\text{dil}}}\right)^n} \qquad (2.2\text{-}3 \ \& \ 2.2\text{-}4)$$

Regrouping terms in eq 2.2-4 and substituting in eq 2.2-3 reveals:

$$[\mathrm{M}]_{\text{after}} \approx \frac{\frac{1}{f_{\text{dil}}}}{\left(\frac{1}{f_{\text{dil}}}\right)^n} \left(\frac{[\mathrm{ML}_n]}{\beta_n [\mathrm{L}]^n}\right) \approx f_{\text{dil}}{}^{n-1} \left(\frac{[\mathrm{ML}_n]}{\beta_n [\mathrm{L}]^n}\right) \approx f_{\text{dil}}{}^{n-1} \, [\mathrm{M}]_{\text{before}} \qquad (2.2\text{-}5)$$

which rearranges to:

$$\frac{[\mathrm{M}]_{\text{after}}}{[\mathrm{M}]_{\text{before}}} \approx f_{\text{dil}}{}^{n-1} \qquad (2.2\text{-}6)$$

Because the dilution factor f_{dil} can only be greater than 1, eq 2.2-6 returns a value that can also only be greater than 1 whenever higher stoichiometries are in place. The free metal concentration in the "after" dilution state is always larger by a multiplicative factor, $f_{\text{dil}}{}^{n-1}$. For example, a 10-fold dilution in a system dominated by a 1:2 metal-ligand complex (*i.e.*, n=2) results in:

$$\frac{[\mathrm{M}]_{\text{after}}}{[\mathrm{M}]_{\text{before}}} \approx 10^{2-1} = 10 \qquad (2.2\text{-}7)$$

The $f_{\text{dil}}{}^{n-1}$ multiplicative factor for $[\mathrm{M}]_{\text{before}}$ is only part of the behavior of anti-buffering. Not only has the concentration of M increased, but the increase has happened during a dilution event in which other species have decreased by a factor of $1/f_{\text{dil}}$.

The two effects are cumulated for a dilution procedure into an anti-buffering effect (ABE), the product of the two contributions:

$$\text{ABE} = \Delta C \times \Delta[\text{M}] \qquad (2.2\text{-}8)$$

Where

$$\Delta C = \frac{C_{\text{before}}}{C_{\text{after}}} \quad \text{and} \quad \Delta[\text{M}] = \frac{[\text{M}]_{\text{after}}}{[\text{M}]_{\text{before}}} \qquad (2.2\text{-}9 \text{ \& } 2.2\text{-}10)$$

Long before the anti-buffering capacity is reached, ABE is occurring to its maximum degree. Its magnitude under these conditions would be

$$\text{ABE} = f_{\text{dil}} \times f_{\text{dil}}^{n-1} = f_{\text{dil}}^{n} \qquad (2.2\text{-}11)$$

As the anti-buffering capacity is neared, however, the value of ABE eventually diminishes to one.

Table 2.2-1 lists the maximum value of ABE for an order of magnitude dilution (ΔC = 10) with various dominant stoichiometries. It indicates for an exclusively 1:1 system that the multiplicative factor f_{dil}^{n-1} = 1, so no change in concentration is present despite the 10-fold dilution. This is the traditional metal ion buffering that was described in the previous chapter. For systems with higher stoichiometries, the multiplicative factor is greater than 1; an exponential increase in free metal concentration will occur with dilution. For a 1:2 complex system (n = 2), the concentration will be 10 times larger (*i.e.,* f_{dil}^{2-1} = 10). When combined with the ΔC of 10, it yields an overall ABE of 100. For a 1:3 complex system (n = 3), the concentration will be 100 times larger and lead to an overall ABE of 1000.

Table 2.2-1. Maximum magnitude of the anti-buffering effect (ABE) for an order of magnitude dilution (ΔC = 10).

Dominant Stoichiometry	***n***	**Multiplicative Factor f_{dil}^{n-1}**	**Anti-Buffering Effect ABE = ΔC x Δ[M]**
1:1	1	1	10
1:2	2	10	100
1:3	3	100	1000
1:4	4	1000	10,000

2.2.3 The Chemical Model for the Cu^{2+}-Ethylenediamine System

The aqueous equilibrium chemistry that occurs in a metal complexation titration is more complicated than that in a simple Brønsted-Lowry acid-base system. There are competing reactions for both the metal ion and ligand components. Because these reactions are being conducted in aqueous solution, there is always competition for the metal ion between the ligand of interest and the ever-present OH^- ligand of the water itself. In a similar fashion, there is always competition for the ligand's binding sites between the metal ion and the ever-present H_3O^+ of the water. Additionally, if the pH gets sufficiently high, there is also the possibility of metal hydroxide precipitation. Because of these competing processes, metal complexation titrations are often done at constant pH to reduce the variables in the system. That practice is followed here.

A sample metal-ligand system will be useful for describing the competitive reactions. The initial system explored here consists of Cu^{2+} as the metal ion and ethylenediamine, $NH_2CH_2CH_2NH_2$, a well-studied bidentate ligand that is often abbreviated as "en". Below are details regarding the four classes of reactions and the notational scheme used for their equilibrium constants.

Complexation reactions: There are three Cu-en complexes that can form. The formation of the complexes can be written as a set of step-wise reactions:

$$Cu^{2+} + en \rightleftharpoons Cu(en)^{2+} \qquad \mathcal{K}_{F1} = 10^{10.47} \qquad (2.2\text{-}12)$$

$$Cu(en)^{2+} + en \rightleftharpoons Cu(en)_2^{2+} \qquad \mathcal{K}_{F2} = 10^{9.20} \qquad (2.2\text{-}13)$$

$$Cu(en)^{2+} + en \rightleftharpoons Cu(en)_3^{2+} \qquad \mathcal{K}_{F3} = 10^{0.69} \qquad (2.2\text{-}14)$$

For concise coding, the Complexation TOPOS software uses overall reactions as opposed to step-wise reactions. Here are the equivalent thermodynamic expressions with their β notational scheme:

$$Cu^{2+} + en \rightleftharpoons Cu(en)^{2+} \qquad \beta_1 = \mathcal{K}_{F1} = 10^{10.47} \qquad (2.2\text{-}15)$$

$$Cu^{2+} + 2\,en \rightleftharpoons Cu(en)_2^{2+} \qquad \beta_2 = \mathcal{K}_{F1} \times \mathcal{K}_{F2} = 10^{(10.47+9.20)} = 10^{19.67} \qquad (2.2\text{-}16)$$

$Cu^{2+} + 3\ en \rightleftharpoons Cu(en)_3^{2+}$ $\beta_3 = \mathcal{K}_{F1} \times \mathcal{K}_{F2} \times \mathcal{K}_{F3} = 10^{(10.47+9.20+0.69)} = 10^{20.36}$ (2.2-17)

As we discuss the shifts from one copper species to another, we will use γ coefficients to quantify how much is present in each form. These are analogous to the α coefficients used in acid-base species distribution diagrams. For simplicity, we are eliminating the H_2O molecules that occupy other positions in the coordination sphere. In actuality, Cu^{2+} is more realistically represented as $Cu(H_2O)_6^{2+}$. We are also ignoring hydroxy complexes in the γ coefficients.

γ_0 represents the fraction present as free copper ion, *i.e.,* Cu^{2+}

$$\gamma_0 = \frac{\left[Cu^{2+}\right]}{\left[Cu^{2+}\right]+\left[Cu(en)^{2+}\right]+\left[Cu(en)_2^{2+}\right]+\left[Cu(en)_3^{2+}\right]} \quad (2.2\text{-}18)$$

γ_1 represents the fraction of $Cu(en)^{2+}$

$$\gamma_1 = \frac{\left[Cu(en)^{2+}\right]}{\left[Cu^{2+}\right]+\left[Cu(en)^{2+}\right]+\left[Cu(en)_2^{2+}\right]+\left[Cu(en)_3^{2+}\right]} \quad (2.2\text{-}19)$$

γ_2 represents the fraction of $Cu(en)_2^{2+}$

$$\gamma_2 = \frac{\left[Cu(en)_2^{2+}\right]}{\left[Cu^{2+}\right]+\left[Cu(en)^{2+}\right]+\left[Cu(en)_2^{2+}\right]+\left[Cu(en)_3^{2+}\right]} \quad (2.2\text{-}20)$$

γ_3 represents the fraction of $Cu(en)_3^{2+}$

$$\gamma_3 = \frac{\left[Cu(en)_3^{2+}\right]}{\left[Cu^{2+}\right]+\left[Cu(en)^{2+}\right]+\left[Cu(en)_2^{2+}\right]+\left[Cu(en)_3^{2+}\right]} \quad (2.2\text{-}21)$$

For pedagogic clarity, complexes with protons occupying some ligand sites, *e.g.*, $CuH_x(en)_y^{2+x}$, additional higher stoichiometries, and polynuclear metal complexes, *e.g.,* $Cu_2(en)_x^{4+}$ have been omitted. Also omitted are activity effects, assuming the system is maintained at a constant ionic strength and that any differences between concentrations and activities would simply be a small, uniform scalar factor over the complete composition grid. Even without a constant ionic strength, the change in the activity coefficient for Cu^{2+} over the 0.001 M – 0.1 M range of concentrations is a factor of 2.14. The ABE over the same range is 1000. Ion pair formation is also neglected. All constants used in this chapter are from Martel *et al. NIST Critical Stability Consta*nts *of Metal Complexes Database 46*.[7]

Protonation of ligand reactions: Acid-base chemistry is traditionally treated as loss of protons. Given the structure of our computer program, it is more convenient to write these in the reverse direction. This is equivalent to forming "hydrogen complexes" of the ligands. All that needs to be done is switch the order of constants and the sign on their p$\mathcal{K}_a$ values. The last proton lost is the same as the first proton "complexed". These, too, are done as overall constants, not step-wise constants. Here is a comparison of the standard $\mathcal{K}_a$ notation and the β_H notation used in our program:

Step-wise dissociation of protonated ligand:

$$H_2en^{2+} + H_2O \rightleftharpoons H_3O^+ + Hen^+ \qquad \mathcal{K}_{a1} = 10^{-6.848} \qquad (2.2\text{-}22)$$

$$Hen^+ + H_2O \rightleftharpoons H_3O^+ + en \qquad \mathcal{K}_{a2} = 10^{-9.928} \qquad (2.2\text{-}23)$$

Overall protonation of ligand reactions:

$$H^+ + en \rightleftharpoons Hen^+ \qquad \beta_{H1} = 10^{9.928} \qquad (2.2\text{-}24)$$

$$2\,H^+ + en \rightleftharpoons H_2en^{2+} \qquad \beta_{H2} = 10^{(9.928+6.848)} = 10^{16.776} \qquad (2.2\text{-}25)$$

Metal Hydrolysis Reactions: Whenever metal ions are dissolved in water, there is a possible interaction with OH^- as a ligand. Complexes formed with OH^- really represent a replacement of an H_2O molecule in the coordination sphere

of the aqueous ion. As stated above, we are ignoring the coordination water in our formulas.

$$Cu^{2+} + OH^- \rightleftharpoons Cu(OH)^+ \qquad \beta_{OH1} = 10^{6.50} \qquad (2.2\text{-}26)$$

$$Cu^{2+} + 2\ OH^- \rightleftharpoons Cu(OH)_2^0 \qquad \beta_{OH2} = 10^{11.80} \qquad (2.2\text{-}27)$$

$$Cu^{2+} + 3\ OH^- \rightleftharpoons Cu(OH)_3^- \qquad \beta_{OH3} = 10^{14.50} \qquad (2.2\text{-}28)$$

$$Cu^{2+} + 4\ OH^- \rightleftharpoons Cu(OH)_4^{2-} \qquad \beta_{OH4} = 10^{15.60} \qquad (2.2\text{-}29)$$

Precipitation: For our Cu^{2+} system, we also need to be alert for the possibility of hydroxide precipitates forming. This reaction is characterized with a solubility product constant, $\mathcal{K}_{sp}$.

$$Cu^{2+} + 2\ OH^- \rightleftharpoons Cu(OH)_2(s) \qquad \mathcal{K}_{sp} = 10^{-19.32} \qquad (2.2\text{-}30)$$

The overall scheme of the chemical model for the four interacting reactions in Cu^{2+}-en system is captured as Figure 2.2-1

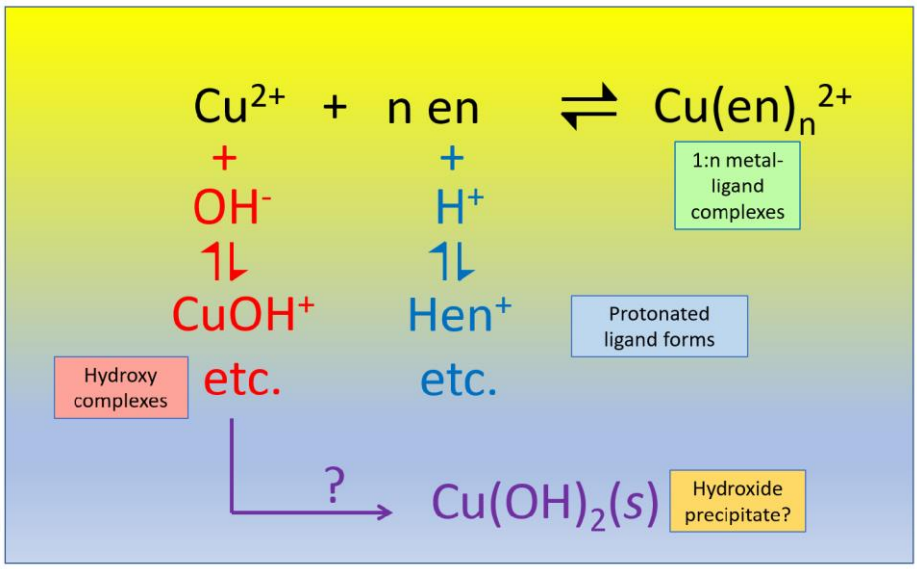

Figure 2.2-1. A simplified diagram for the chemical model of the Cu^{2+}-en sample system.

2.2.4 2-D Complexometric Titration Curves

The 3-D trend surfaces that display the anti-buffering phenomenon are comprised of a collection of 2-D complexometric titration curves at systematically spaced dilutions. Thus, it is helpful to review what each of the titration slices looks like before assembling them into a topo. This section reviews the traditional 2-D curves for a ligand-into-metal titration. It permits an examination of the importance of individual species during the course of the procedure.

The sample 2-D slice examined here is for the titration of a 1.0 M solution of Cu^{2+} with a 1.0 M solution of ethylenediamine, en (Figure 2.2-2). These concentrations are higher than would normally be used in practice. Because our topo surfaces encompass as wide a range of solution compositions as possible, the front of our surfaces is always the 1.0 M slice. For this titration, we are fixing the pH of the system at 5.50. This is sufficiently high in OH^- to cause some precipitation of $Cu(OH)_2(s)$ at the beginning which will persist until sufficient en has been added to bind much of the copper in aqueous complexes. The y-axis is log $[Cu^{2+}]$ rather than pCu^{2+} as is often used. With this convention, an upward trend on the log $[Cu^{2+}]$ axis represents an increase in concentration.

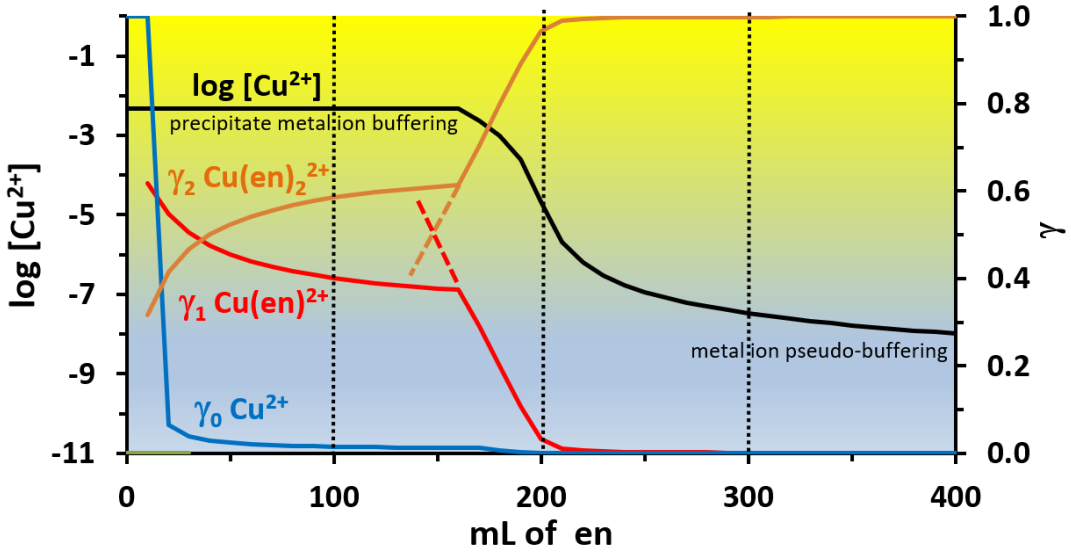

Figure 2.2-2. Log $[Cu^{2+}]$ curve (black) and species distribution curves (blue, red and brown) for the titration of 100 mL of 1.0 M Cu^{2+} with 1.0 M en at pH 5.50. Equivalence points are indicated by the dashed vertical lines.

The black trace of Figure 2.2-2 shows the complexometric titration curve. Its shape is not necessarily what is typically seen in titration studies. At first, the plot of log [Cu^{2+}] is completely flat. This is a result of precipitate metal ion buffering that is controlled by the presence of $Cu(OH)_2(s)$. As long as there is some solid present, the $\mathcal{K}_{sp}$ dictates the value of [Cu^{2+}].

$$\left[Cu^{2+}\right] = \frac{\mathcal{K}_{sp}}{\left[OH^-\right]^2} = \frac{\mathcal{K}_{sp}}{\left(\frac{\mathcal{K}_w}{10^{-pH}}\right)^2} = \frac{10^{-19.32}}{\left(\frac{10^{-14.01}}{10^{-5.50}}\right)^2} = 4.69 \times 10^{-3}\ \mathrm{M} \qquad (2.2\text{-}31)$$

Note the black trace starts at log [Cu^{2+}] = log (4.69×10^{-3}) = -2.33.

As the titrant and analyte are at the same starting concentration, the equivalence points for the three stoichiometries of complexes will be spaced at equal 100-mL intervals – 100, 200 and 300 mL – as depicted by dashed vertical lines in the figure. Despite that there are three possible stoichiometries (a 1:1 with log β_1 = 10.47, a 1:2 with log β_2 = 19.67, and a 1:3 with log β_3 = 20.36), only one break is exhibited in the log [Cu^{2+}] plot. The first equivalence point at 100 mL is suppressed by precipitate metal ion buffering and never seen. The second equivalence point at 200 mL lands near the midpoint of the drop from the initial plateau to the final lower level. The third equivalence point causes no visible manifestation on the log [Cu^{2+}] curve because the 0.69 log unit stepwise constant for the 1:3 stoichiometry is too small. A stepwise constant must be at least 3.0 to be seen. Once the single break has occurred, the value of log [Cu^{2+}] drops fairly slowly in what could be called pseudo-buffering, a situation in which an excess of titrant slowly approaches its undiluted value.

The copper speciation is shown by the three γ traces of Figure 2.2-2. The fraction of 1:3 $Cu(en)_3^{2+}$ is so small, that γ_3 lands on top of the x-axis and is not included. (We are ignoring any $Cu(OH)_x(aq)$ species for pedagogical clarity.) Initially, before any en has been added, all Cu^{2+} is present in its free form and γ_0 is equal to 1.0. With the addition of en, the 1:1 complex begins to form. But the 1:2 complex is so much stronger that it also is forming in the early stages of the titration. Shortly after the 30-mL data point, γ_2 crosses over the γ_1 curve. Normally, one would expect the crossover to occur halfway between the first and second equivalence points. The skewing of the crossover between γ_1 and γ_2 is

caused by the interaction between the $Cu(OH)_2(s)$ and the complexes. Without the precipitate metal ion buffering, we have extrapolated the shape of the γ_1 and γ_2 curves with dashed lines. One can see that the crossover point would have been around 150 mL.

Once all of the $Cu(OH)_2(s)$ precipitate is gone, the γ_1 and γ_2 traces proceed, as expected, to values of essentially 0.0 and 1.0, respectively. As mentioned earlier, γ_3 never is large enough to be seen above the x-axis at this scale. An examination of the γ_3 data array reveals that the maximum value $[Cu(en)_3^{2+}]$ attains is a mere 3.14×10^{-6} M, thus γ_3 is miniscule.

Concentrations, rather than γ values are plotted in Figure 2.2-3. This provides a bit more detail in the speciation that is occurring in the precipitate metal ion buffering region. As was true in Figure 2.2-2, there are no visible changes in the curves at either the first or third equivalence points. The system is dominated by the 1:2 complex over most of the mL of en axis which reaches its maximum at the second equivalence point.

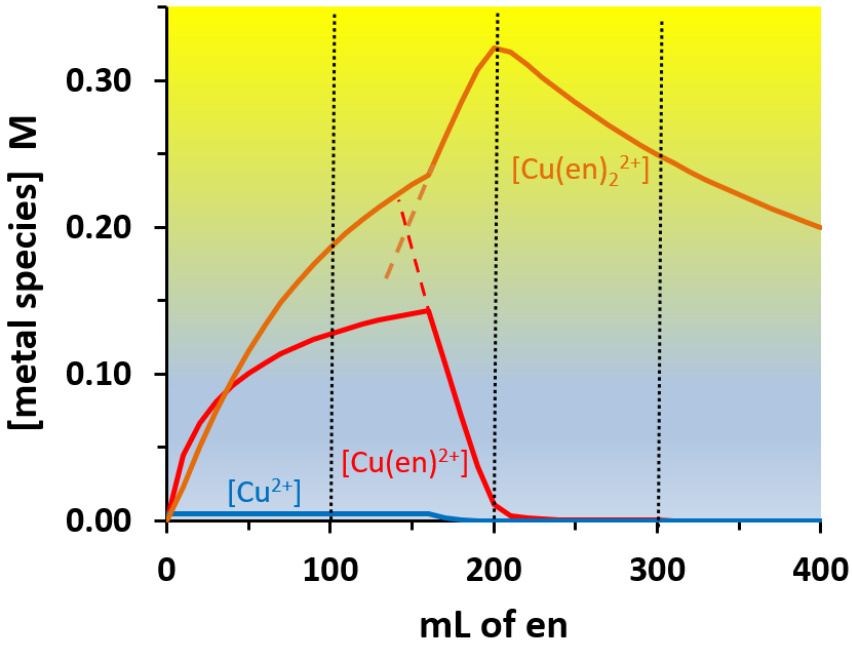

Figure 2.2-3. Cu species concentrations for the titration of 100 mL of 1.00 M Cu^{2+} with 1.00 M en at pH 5.50.

2.2.5 Metal Ion Anti-Buffering Illustrated: The Log [Cu^{2+}] 3-D Topo

Metal ion anti-buffering has probably been overlooked by earlier investigators because dilution as an experimental variable has not been extensively explored. In adding a dilution axis to metal-ligand titrations, anti-buffering is unmistakably evident. Whenever higher stoichiometries dominate a complexation system, the concentration of free metal cation can dramatically INCREASE as the system undergoes DILUTION. This is counterintuitive. To our knowledge, this phenomenon has not previously been described in the literature. Data supporting this effect, however, appeared as long ago as 1970.[8] Figure 6.11 of Stumm and Morgan's seminal book on aquatic chemistry shows plots of Cu^{2+} as a function of dilution. The trace for their Cu^{2+}-NH_3 system shows an increase in [Cu^{2+}] of ~100 times as the solution undergoes a dilution of ~100 times, an ABE of about 10,000. Though there was an increase in free metal concentration with dilution, they did not mention its significance.

A log [Cu^{2+}] surface for the Cu^{2+}- en titration-dilution grid at pH 5.50 clearly reveals anti-buffering behavior (Figure 2.2-4). As above, log [Cu^{2+}] is used rather than pCu^{2+}. Thus, an upward trend on the log [Cu^{2+}] axis represents an increase in concentration. For purposes of visual interpretation, the data are presented as both a 3-D wire-frame surface (Panel a) and as a contour map (Panel b).

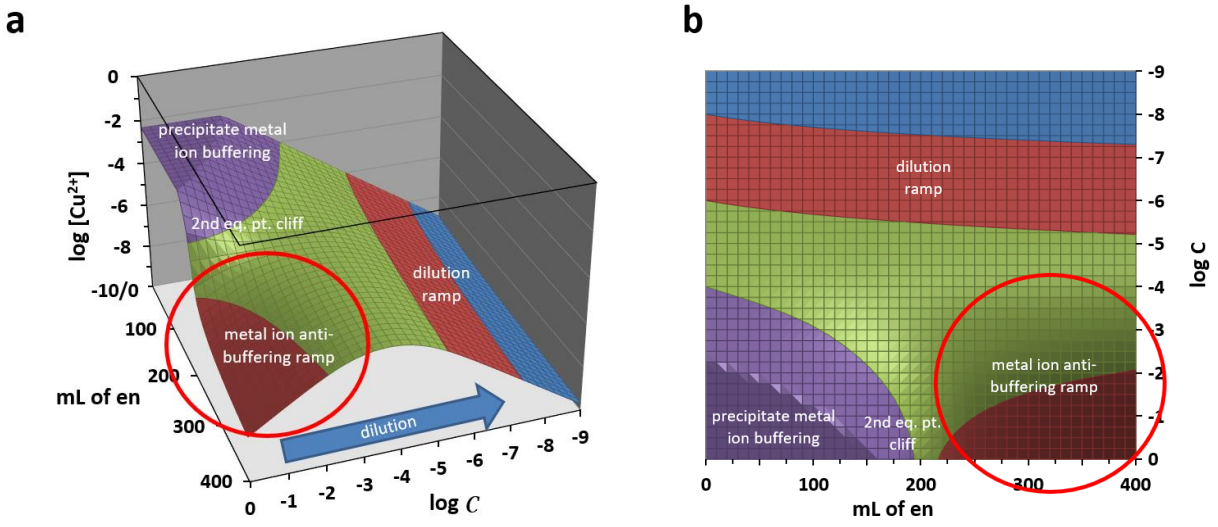

Figure 2.2-4. Log [Cu^{2+}] surface for 100 mL of Cu^{2+} titrated with an equimolar solution of en at pH 5.50. The metal ion anti-buffering region is circled. a) wire-frame; b) contour map.

The topo surface for log [Cu^{2+}] exhibits four regions. First, prior to 160 mL, a flat "precipitate metal ion buffering" plateau is seen indicating that $Cu(OH)_2(s)$ is present. Next, an "equivalence point cliff" is centered at 200 mL, the second equivalence point. The cliff height diminishes in the dilution direction until it becomes indistinct around log C = -3.5. Beyond the equivalence point cliff, circled in red for emphasis, is the third surface region – the "metal ion anti-buffering ramp". It runs at a 45° upward slope (*i.e.,* +1) in the dilution direction. This seems contrary to what should happen as a system is diluted! Finally, when the log C = -3.5 line is crossed, the fourth region is a broad "dilution ramp" descending at a 45° angle across the entire width of the topo. A ramp sloping downward at 45° (*i.e.*, a -1 slope) in the log C direction is the normal concentration behavior observed when a species undergoes dilution.

Because metal ion anti-buffering is a new and previously undescribed concept, it warrants a detailed discussion. First, it needs to be distinguished from the more familiar metal ion buffering [9-11] that was the principal thrust of Chapter 2.1. Figure 2.2-5 provides a comparative topo surface that exhibits "precipitate metal ion buffering" and "mass action metal ion buffering" but no "mass action metal ion anti-buffering". A visual comparison between Figure 2.2-4a and Figure 2.2-5 should make the difference between buffering and anti-buffering easy to see. Note that with traditional metal ion buffering, there is a flat plateau occupying the topo surface beyond the equivalence point cliff, not an upward-sloping 45° ramp.

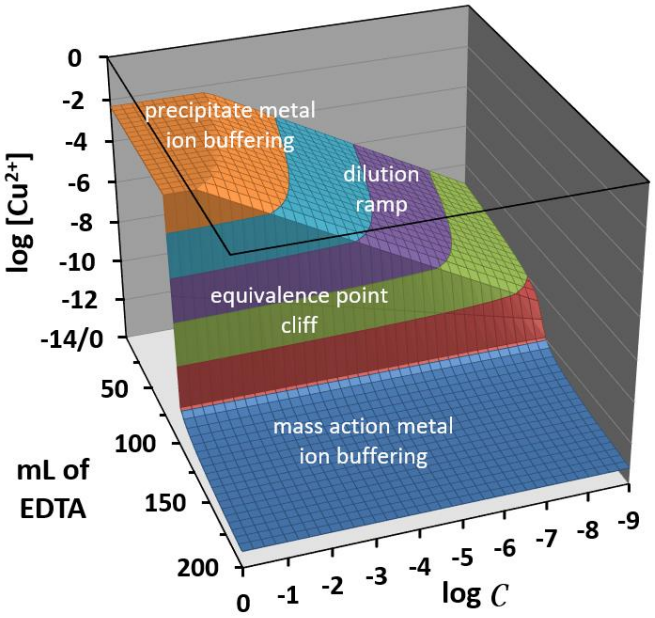

Figure 2.2-5. A comparative log [Cu^{2+}] surface for 100 mL of Cu^{2+} being titrated with an equimolar EDTA solution at pH 5.50.

Anti-buffering only occurs in the post-equivalence point regions where excess free ligand is present and higher complexes dominate the system. Using the pH 5.5 Cu^{2+}-en surface of Figure 2.2.4, the extent of anti-buffering can be quantified. Note that both axes involved in this calculation are logarithmic, so the change is substantial in magnitude. Anti-buffering occurs over the upward trending region of the surface that starts at log C = 0.0 and continues until log C = -3.75. This range corresponds to dilution by a factor of $\Delta C = 10^{3.75}$ = 5,623. Across this same range, the value of log [Cu^{2+}] rises from -7.984 to -5.313. This is a $\Delta[Cu^{2+}] = 10^{(7.984-5.313)} = 10^{2.671}$ = 469-fold increase in concentration. Taken together, the anti-buffer effect (ABE) = ΔC x $\Delta[Cu^{2+}]$ = 5,623 x 469 = 2.64 x 10^6. Thus, the concentration of free Cu^{2+} is 2.64 million times higher than dilution of the system would yield in other circumstances. At log C = -3.75 the anti-buffering capacity of the system has been depleted. Normal dilution behavior is exhibited beyond this point such that a dilution ramp now extends across the entire width of the surface.

What causes metal ion anti-buffering? It is only observed when diluting systems of aqueous metal complexes in which stoichiometries higher than 1:1 are dominant. It also requires that excess free ligand conditions exist and that the overall protonation constants for the ligand are less than the overall formation constant for a higher complex. For the Cu^{2+}-en system, the first protonation constant is log β_{H1} = 9.928 while the overall formation constants for the Cu^{2+}-en complexes are log β_1 = 10.47, log β_2 = 19.67 and log β_3 = 20.36. For the Cu^{2+}-en system, the 1:2 complex, $Cu(en)_2^{2+}$, is dominant. Very little of the 1:3 complex ever forms. When a system with these properties is diluted, some of the dominant higher stoichiometry complex will dissociate through the Law of Mass Action.

$$Cu(H_2O)_6^{2+} + 2\ en \rightleftharpoons Cu(en)_2(H_2O)_2^{2+} + 4\ H_2O$$

Shifts left with addition of dilution H_2O

(2.2-32)

The addition of dilution water is equivalent to adding more product H_2O and, per le Chatelier's Principle, the equilibrium will shift to the left causing some dissociation to occur. The dissociation shown in eq 2.2-32 happens in two sequential steps, but here it is combined into an overall end result. The metal ion

that is released through this dissociation will be so significant compared to what was there prior to dilution, that the resulting free metal ion concentration will rise.

While the change in trace free metal ion concentration is substantial, the loss of $Cu(en)_2^{2+}$ and gain in free en are tiny compared to their total amounts. The change in these two species' concentrations, therefore, is dominated by the 10-fold dilution drop. Table 2.2-2 reveals modeled quantitative details about the effects of a 10-fold dilution step on the front-edge slice of Figure 2.2-4. A 10-fold dilution, when mL of en = 400, will take log C from 0.00 to -1.00 (*i.e.*, 1.00 M to 0.100 M). Values for $[Cu^{2+}]$, [en], $[Cu(en)^{2+}]$, $[Cu(en)_2^{2+}]$ both before and after the dilution step are listed.

Table 2.2-2. Before and after values for selected species that accompany a 10-fold dilution in the Cu^{2+}-en system at pH 5.50, mL of en = 400 mL and C goes from 1.00 M to 0.100 M (*i.e.*, $\Delta C = 10$).

Species:	$[Cu^{2+}]$ / M	[en] / M	$[Cu(en)^{2+}]$ / M	$[Cu(en)_2^{2+}]$ / M
Before:	1.08×10^{-8}	6.42×10^{-7}	1.97×10^{-4}	2.00×10^{-1}
After:	1.02×10^{-7}	6.44×10^{-8}	1.94×10^{-4}	1.98×10^{-2}
Ratio of After/Before:	9.83 (10-fold dilution + dissociation gains)	0.1004 (10-fold dilution + dissociation gains)	0.986969 (10-fold dilution – 1:1 dissociation losses + 1:2 dissociation gains)	0.0991 (10-fold dilution – dissociation losses)
Approximate change:	~10-fold INCREASE	~10-fold DECREASE	~ NO CHANGE	~10-fold DECREASE

The concentration of the 1:2 complex, $Cu(en)_2^{2+}$, drops by slightly more than a factor of ten. Not only did it get diluted, but also 1.31% dissociated. One product of its dissociation was 1:1 complex. Note that the concentration of 1:1 $Cu(en)^{2+}$ stayed almost the same, 1.97×10^{-4} M before to 1.94×10^{-4} M afterwards.

Dissociation contributions from the 1:2 complex were essentially balanced by dissociation losses of the 1:1 complex. The concentration of free en dropped by not quite a factor of 10. A small amount of en was released through dissociation of both the 1:2 and 1:1 complexes. This added free en was small compared to what was already there in excess. It increased by a factor of 0.312% relative to what was present before dilution. The small amount of dissociation, however, did release a comparatively large amount of Cu^{2+} ion. $[Cu^{2+}]$ rose from 1.08×10^{-8} M to 1.02×10^{-7}, an almost 10-fold rise.

To reiterate, the system was diluted by a factor of 10 and the free metal concentration went up by a factor of 9.83. Computationally the anti-buffering effect that results is ABE = ΔC x $\Delta[Cu^{2+}]$ = 10 x 9.83 = 98.3 ≈ 100 = 10^2.

A predominant metal species plot confirms the requirements for the occurrence of anti-buffering (Figure 2.2-6). This plot provides visual evidence that anti-buffering happens when the system is dominated by a higher stoichiometry complex. The fraction of Cu in each form is symbolized with γ notation. The fraction of free Cu^{2+} is γ_0, the fraction of $Cu(en)^{2+}$ is γ_1, and that of $Cu(en)_2^{2+}$ is γ_2. Here, the fraction of metal in the predominant form is plotted above each grid point. It is useful to view both the wire-frame and contour versions of the surface to aid in the interpretation of its features. The wire-frame topo orientation has been rotated to optimize visualization of the anti-buffering boundary ridge.

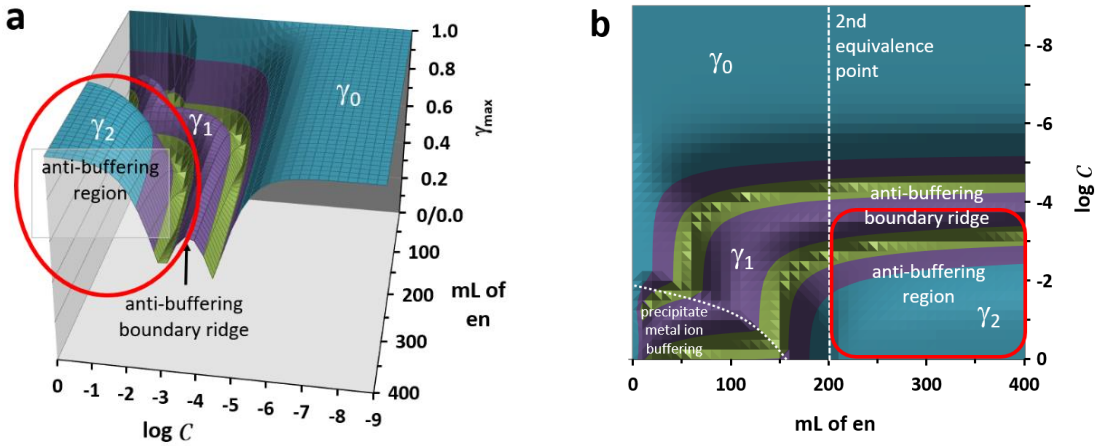

Figure 2.2-6. The predominant metal species surface for 100 mL of Cu^{2+} being titrated with an equimolar en solution at pH 5.50 with the metal ion anti-buffering region encircled. a) wire frame; b) contour map.

The dashed line in Figure 2.2-6b, the second equivalence point at 200 mL, marks the vertical anti-buffering boundary on the map. This represents the point where excess free en and $Cu(en)_2^{2+}$ emerge as major species. The map's horizontal boundary is a bit more complicated. Anti-buffering persists until log C = -3.75. This is the top of the γ_1 ridge. The rise in log $[Cu^{2+}]$ is fastest with dilution when γ_2 predominates, but it continues to rise at a slower rate as the remaining $Cu(en)_2^{2+}$ dissociates into $Cu(en)^{2+}$. Were the $Cu(en)_2^{2+}$ complexes not present, the $Cu(en)^{2+}$ would only established mass action metal ion buffering, not anti-buffering, in this region. The combination of anti-buffering from the 1:2 complex and the buffering from the 1:1 complex leads to a slowing rise in metal ion concentrations. When the metal ion buffer capacity of the 1:1 complex is finally encountered through dilution, metal ion buffering ceases and a descending dilution ramp begins to form. Metal ion dilution ramps are present wherever γ_0 is the predominant form.

2.2.6 The Effect of pH on Anti-Buffering

The extent of anti-buffering is dictated by the pH at which the system is maintained. As the system pH moves to lower values, the extent of anti-buffering in the dilution direction will decrease. As the system pH increases, the extent of the anti-buffering rises. Figure 2.2-7 shows dilution curves for log $[Cu^{2+}]$ in the 400-mL slice of the Cu^{2+}-en system at three pHs – 5.0, 5.5 and 6.0.

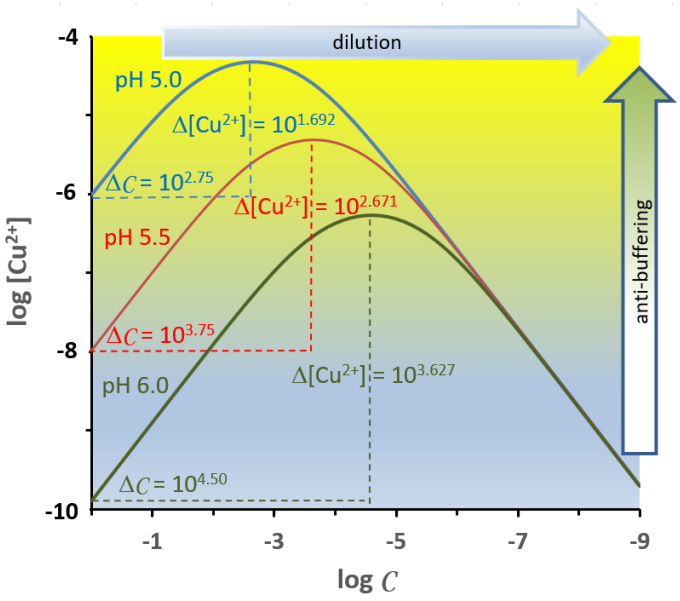

Figure 2.2-7. The extent of anti-buffering in the Cu^{2+}-en system for the 400-mL slice at pHs of 5.0, 5.5 and 6.0.

At lower pH values, H_3O^+ becomes more competitive for ligand sites. In other words, the conditional β_xs for the Cu^{2+}-en complexes are smaller. Note that the initial log [Cu^{2+}] value is highest at -6.017 for pH 5.00 and lowest at -9.906 for pH 6.00. There is more Cu^{2+} ion in solution at pH 5.00 because more ligand sites are occupied by protons. At the same time, the anti-buffering boundary moves further to the right on the log C axis as the pH is raised. At higher pHs the complexes are stronger (bigger conditional β_xs), so more dilution is required to drive their dissociation via the mass action effect. The boundary moves from log C = -2.75 at pH 5.0 to log C = -4.75 at pH 6.0. The overall ABE values for the three pHs are computed in Table 2.2-3. (Note: Resolution of the dilution factor in these calculations is limited to grid-point log C values.)

Table 2.2-3. Calculation of the anti-buffering effect (ABE) for the 400-mL slice of the three Cu^{2+}-en systems in Figure 2.2-7.

pH	ΔC	Δ[Cu^{2+}]	ABE = ΔC x Δ[Cu^{2+}]
5.00	$10^{2.75}$ = 562	$10^{(6.017-4.325)}$ = 49.2	27,700
5.50	$10^{3.75}$ = 5,623	$10^{(7.984-5.313)}$ = 469	2.64 x 10^6
6.00	$10^{4.50}$ = 31,623	$10^{(9.906-6.279)}$ = 4,266	1.34 x 10^8

If the pH goes much beyond 6.00, precipitation of $Cu(OH)_2(s)$ becomes more pronounced and begins to erode into the equivalence point cliff, but the anti-buffering behavior will continue to expand both in magnitude and duration under dilution.

2.2.7 Experimental Confirmation of Anti-Buffering in the Cu^{2+}-en system

Having discovered the existence of metal ion anti-buffering through computer modeling, it was a logical next step to confirm its presence experimentally. The procedure was performed on a solution whose composition placed it in the anti-buffering region of the titration-dilution composition grid. Unlike the modeling that ignores activity effects for pedagogical ease, activity

corrections were applied to the experimental measurements so that laboratory data could be compared to modeled data. A constant ionic strength of 0.1 M was maintained during the dilution. Metal and ligand concentrations in our starting solution were well below this value.

A basic potentiometric apparatus was built to follow the activity of free Cu^{2+} ions as a Cu^{2+}-en mixture was diluted.[12] The experimental design and measurement equipment details are found in a supplementary file. The starting solution contained a ten-fold excess of en over Cu^{2+}, 0.031 M en to 0.0031 M Cu^{2+}. This placed it well into the excess ligand region. Dilution was done in five stages with water at pH 6.0 that had been deionized, degassed and supplemented with KNO_3 ionic strength adjustor (ISA) to 0.1 M. Figure 2.2-8 shows the experimental results compared to the modeled values.

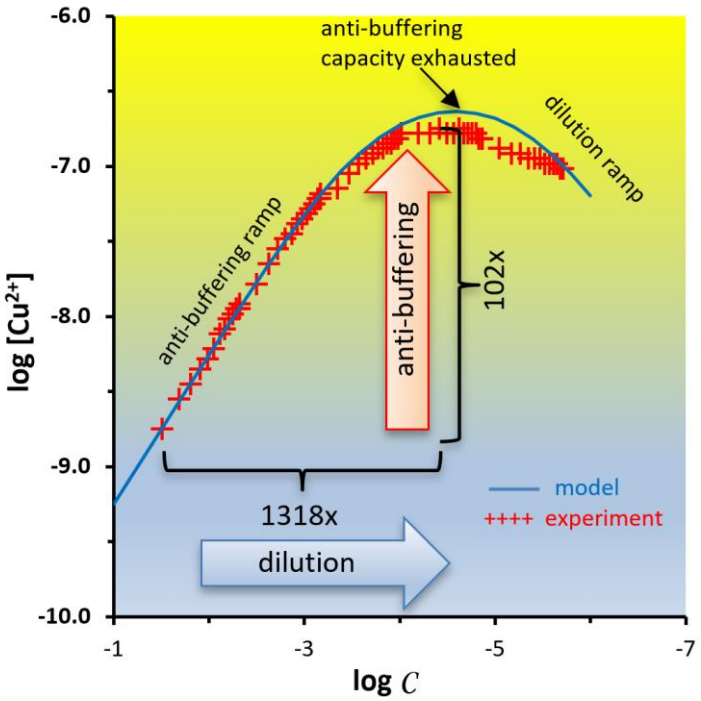

Figure 2.2-8. Experimental confirmation showing an anti-buffering effect of ~135,000 for a 1318-fold dilution of 0.031 M en and 0.0031 M $Cu(NO_3)_2$ at pH = 6.0.

Because Anti-Buffering TOPOS does not incorporate activity effects, the Cu^{2+} values reported for the experiment were converted from activities to concentrations. The total dilution reduced log C from -1.50 to -5.71, equivalent to a $10^{(5.71-1.50)} = 10^{4.21} \approx$ 16,200-fold dilution. A serial procedure was employed to manage this large range in the 400-mL reaction vessel. It required five stages, each of which accomplished a 7-fold dilution. The overall span covered was

sufficient to follow the anti-buffering behavior from the initial point to the highest log [Cu^{2+}] value as the anti-buffering capacity was depleted at log C = -4.62. Thus, the ΔC contribution to the overall anti-buffering effect was $10^{(4.62-1.50)} = 10^{3.12}$ = 1318 times. During this dilution process, the log [Cu^{2+}] value rose from -8.75 to -6.74. This represents an increase in the [Cu^{2+}] of $10^{(8.75-6.74)} = 10^{2.01}$ = 102 times. Combining the two contributions gives an overall observed anti-buffering effect of ABE = 1318 x 102 = 134,896 ≈135,000 times.

Once the anti-buffering capacity of the sample is exhausted at log C = -4.62, the trace for log [Cu^{2+}] begins to descend the dilution ramp beyond the maximum. This descent follows the normal 45° slope that corresponds to the dilution of a species. There are no longer sufficient complexes to dissociate and offset the dilution effect.

2.2.8 Other Systems with Anti-Buffering

Anti-buffering is not unique to the Cu^{2+}–en system. This section presents four other metal-ligand systems that display anti-buffering. The first illustrates anti-buffering in an en system with a different metal ion, namely Ni^{2+}. The other three retain Cu^{2+}, but replace en with different types of ligands.

The log [Ni^{2+}] topo for the Ni^{2+}-en system (Figure 2.2-9) looks quite similar to that of the Cu^{2+}-en system but its equivalence point cliff is more pronounced and extends over a greater range of x-axis values. This is because there is a greater separation between its log β_2 and log β_3. For the Cu^{2+} system the values are 19.47 and 20.36; those for the nickel system are 13.54 and 17.71. The large drop in log [Cu^{2+}] for the Cu^{2+}-en system is essentially over at 200 mL, the second equivalence point. The 1:3 $Cu(en)_3^{2+}$ complex never dominates. With Ni^{2+}-en, the log [Ni^{2+}] remains high until just beyond the 300 mL, third equivalence point. The 1:3 $Ni(en)_3^{2+}$ complex dominates the system beyond 260 mL. With a system dominated by a 1:3 complex, anti-buffering is even more pronounced. Note that the 400-mL dilution slice for Ni^{2+}-en at pH 7.50 exhibits an ABE = 15.1 x 10^6, almost an order of magnitude more than that for Cu^{2+}-en at pH 5.50. The angle of the anti-buffering ramp is also noticeably steeper at the lower end because of the 1:3 complex domination.

Figure 2.2-9. Log [Ni^{2+}] topo for 100 mL of metal ion being titrated with an equimolar solution of en at pH 7.50.

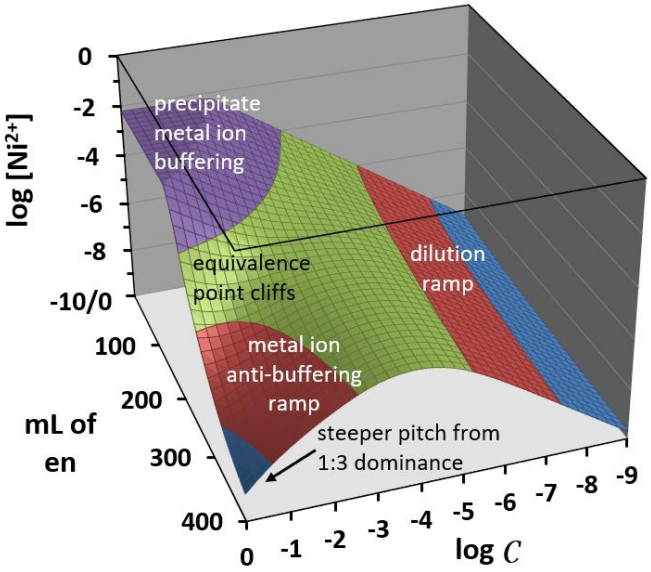

Figure 2.2-10 illustrates anti-buffering for glycine, an amino acid. Most other amino acids have very similar surfaces to this one as the same general complexing groups are present. This system is modeled at pH 7.40, a reasonable physiological pH of blood and cellular cytoplasm. While this pH does create a large precipitate metal ion buffering plateau in excess metal portions of the surface, it also demonstrates significant anti-buffering behavior in excess free ligand conditions. This latter case is likely to be the more common situation in living systems, *i.e.*, a trace amount of a potentially toxic heavy metal in the presence of higher concentrations of common biochemical species. At pH 7.40, the 400-mL dilution slice shows an ABE = 4.77×10^{8}.

Figure 2.2-10. Log Cu^{2+} topo for 100 mL of metal ion being titrated with an equimolar solution of glycine at pH 7.40.

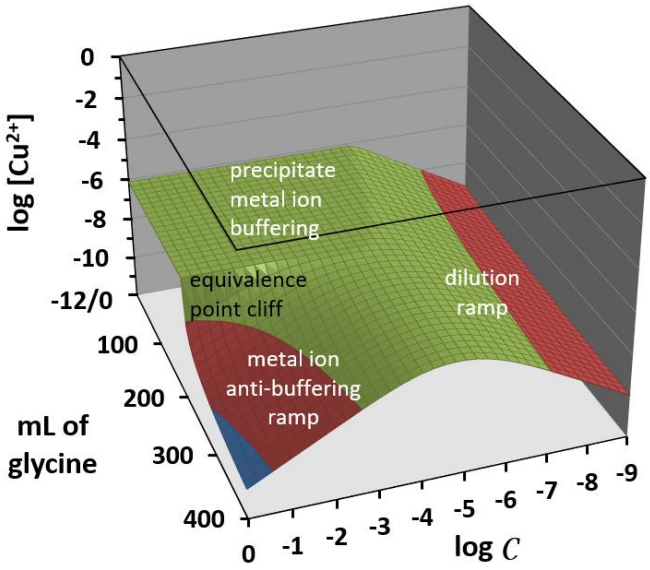

The free metal topo for the Cu^{2+}-3-methylpyridine system at pH 5.50 (Figure 2.2-11) is interesting because complexation is dominated strongly by a 1:3 complex. The overall stability constants used in modeling this surface were log β_1 = 2.7, log β_2 = 4.72, log β_3 = 8.6, and log β_4 = 9. The 1:4 complex is never a significant species. With the 1:3 stoichiometry driving the complexation, we see the major equivalence point cliff for the surface at 300 mL, the third equivalence point. The anti-buffering ramp has an upward slope of 2.0 in the dilution direction as opposed to a slope of 1.0 for a 1:2 complex-dominated system. The ABE = 5.35 x 10^5 is smaller than the previous two systems because the overall log β_3 stability constant of 8.6 is much weaker than the log β_3s of 20.36 and 17.71 for the en systems and the log β_2 of 15.03 for glycine. Hydroxide ion in dilution water can more quickly outcompete the 3-methylpyridine for Cu^{2+}; the log β_{OH2} for $Cu(OH)_2^0$ is 11.80. The anti-buffering behavior in 3-methylpyridine is completely finished by log C = -2.25.

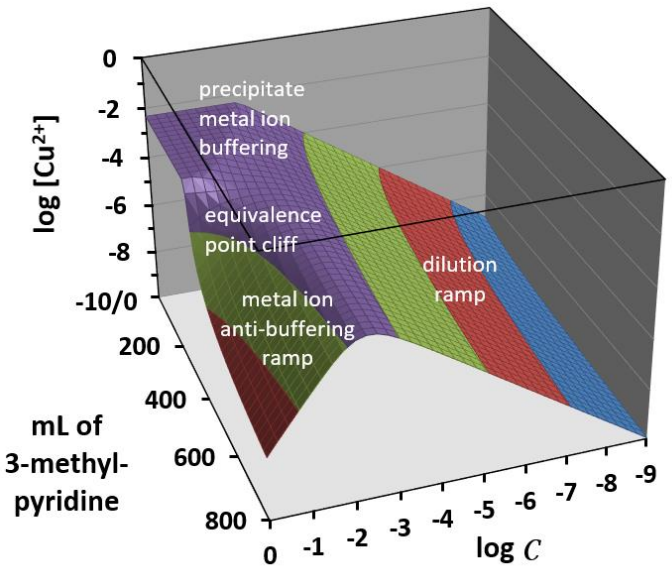

Figure 2.2-11. Log Cu^{2+} topo for 100 mL of metal ion being titrated with an equimolar solution of 3-methylpyridine at pH 5.50.

Finally, Figure 2.2-12 illustrates the Cu^{2+}-1,10-phenathroline system at pH 5.50 in which protonation of the ligand sites is much weaker than the metal complexation. 1,10-phenanthroline has only a single protonation constant, log β_{H1}, of 4.86 while in comparison en has a log β_{H1} of 9.928 and a log β_{H2} of 16.776. The consequence of the weak protonation is anti-buffering behavior that extends over a much larger range in the dilution direction. Note that the maximum on the 400-mL slice is not reached until log C = -7.25. The surface's dilution range does not proceed far enough to establish much of a dilution ramp beyond the anti-

buffering region boundary. As the anti-buffering extends so far in the dilution direction, the overall ABE is 5.21 x 10^{16} for this system! The [Cu^{2+}] is 52.1 quadrillion times larger than would be expected under other circumstances. The ramp has a slope of 2 because the 1:3 complex is predominant over most of the anti-buffering region.

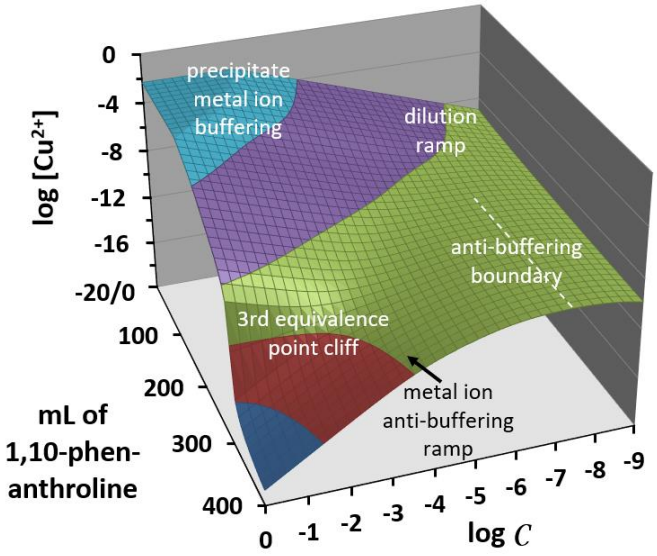

Figure 2.2-12. Log Cu^{2+} topo for 100 mL of metal ion being titrated with an equimolar solution of 1,10-phenanthroline at pH 5.50.

2.2.9 Conclusions

This paper introduces anti-buffering as a new concept in aqueous metal-ligand complexation systems. Through mass action effects, under the right circumstances, the concentration of a free metal ion can dramatically increase as a system is diluted. For anti-buffering to occur:

1. The system to be diluted must have an excess of free ligand over metal;

2. The system must be dominated by a complex with a stoichiometry of at least 1:2; and

3. The overall protonation constants for the ligand must be less than the overall formation constant for a 1:2 or higher complex at the pH of interest.

Many systems satisfying these criteria exist. Experimental studies to confirm its behavior were performed on the Cu^{2+}-ethylenediamine system.

Viewing the surfaces produced by the downloadable Anti-Buffering TOPOS software will help students visualize advanced aqueous equilibrium concepts.

- The surfaces unequivocally introduce metal ion anti-buffering behavior;

- The surfaces clearly distinguish the difference between "mass action metal ion buffering" in systems with only 1:1 complexes and "metal ion anti-buffering" in systems with higher stoichiometries that occurs upon dilution under excess free ligand conditions;

- Species distribution surfaces let students follow the formation of complexes during a titration PLUS the mass action-driven dissociation of the complexes as the system is diluted.

Although the Anti-Buffering TOPOS software is very easy to use, an understanding of its modeling results will require the chemical sophistication of students in junior- or graduate-level courses in analytical chemistry, biochemistry and aquatic chemistry. The concept is so counterintuitive that many of our colleagues were skeptical of its correctness until presented with the experimental data and a careful explanation of its cause.

The speed and ease with which new systems can be visualized makes this a powerful tool for simulation studies. Because it is implemented via Microsoft Excel, no new software need be purchased to run it. With run-times of about five minutes, Anti-Buffering TOPOS is a little slow for "on the fly" calculations by an instructor during a classroom session. It would be easy, however, to do several runs ahead of class and save the results to a new spreadsheet tab for quick recall during a lecture. (Note: that the results need to be pasted into the new tab as "values" in order for the results to be fixed. If pasted in as "formulas", they will change with the next program run.) In a workshop setting, a query from a student about "What would happen to the anti-buffering if…" can easily be addressed with a new run of the program.

2.2.10 Supplementary Files

Six downloadable files are included as additional supplements for this chapter:

1. The downloadable Anti-Buffering TOPOS software implemented as a Microsoft Excel workbook with a table of thermodynamic constants that offers choices of systems to explore. Users can supply their own constants for systems not included in the compilation. Input requirements are complexation constants, ligand protonation constants, metal ion hydroxy complex constants, the stoichiometry and $\mathcal{K}_{sp}$ for metal hydroxide precipitates and the pH of interest.

2. A set of Microsoft PowerPoint slides from which to present a lecture on anti-buffering. Teaching points are highlighted and illustrated with extensively annotated surfaces.

3. Teaching with Anti-Buffering TOPOS is a lesson plan containing itemized learning objectives, with each objective matched to a range of slides in the PowerPoint file. Also included are suggested Anti-Buffering TOPOS workbook activities (homework, prelab, recitation, or peer-led team discussions) and suggestions for coordinated laboratory experiments.

4. A detailed derivation of the mass balance equations that are solved for the equilibrium concentration of free ligand and free metal plus a section on the numerical techniques used to solve them.

5. A full description of our Cu^{2+}-ethylenediamine confirmation experiment that could be used to design a laboratory exercise for an analytical chemistry, physical chemistry, biochemistry, or geochemistry course.

6. An annotated computer code listing for the Anti-Buffering TOPOS macro.

Author Information

Corresponding Author

*E-mail: garon.smith@umontana.edu

ORCID

Garon C. Smith: 0000-0003-0145-8286

Acknowledgements

The project was partially supported by a grant from North South University, Award No. NSU/BIO/CTRGC/47. The authors are grateful to the Department of Chemistry and Biochemistry at the University of Montana for a graduate teaching assistantship and Md Nurul Huda for financial support during the course of these studies. Patrick McCarthy from the Colorado School of Mines was helpful in the initial postulation of anti-buffering behavior.

References

1. Wang, J.; Zeng, L.; Ding, D.; Li, X.; Zhang, H.; Zhao, H.; Fan, J.; Zhang, W.; He, Y. Studies on the Interaction of Achiral Cationic Pseudoisocyanine with Chiral Metal Complexes. *Phys. Chem. Chem. Phys.,* **2011**, *13*, 16741–16747. https://doi.org/10.1039/C1CP20470J
2. Wang, J.; Liu, C.; Ding, D.; Zeng, L.; Cao, Q.; Zhang, H.; Zhao, H.; Li, X.; Xiang, K.; He, Y.; Wang, G. Aggregation of an Anionic Porphyrin with Chiral Metal Complexes and the Competitive Binding Influences of a Surfactant and a Polyelectrolyte. *New J. Chem.,* **2011**, *35*, 1424–1432. https://doi.org/10.1039/C1NJ20193J
3. Liebig, T.; Ruschewitz, U. Supramolecular Polymers with $[Co(en)_3]^{3+}$ Cores (en = ethylenediamine). *Cryst. Growth Des.*, **2012**, *12* (11), 5402–5410. https://doi.org/10.1021/cg3010085
4. Johnson, A.R.; McQueen, T.M.; Rodolfa, K.T. Species Distribution Diagrams in the Copper–Ammonia System: An Updated and Expanded Demonstration Illustrating Complex Equilibria. *J. Chem. Educ*., **2005**, *82* (3), 408-414. https://doi.org/10.1021/ed082p408
5. Muchowska, K.B.; Varma, S.J.; Chevallot-Beroux, E.; Lethuillier-Karl, L.; Li, G.; Moran, J. Metals Promote Sequences of the Reverse Krebs Cycle." *Nat. Ecol. Evol.,* **2017**, *1* (11), 1716-1721. https://doi.org/10.1038/s41559-017-0311-7
6. Hem, J.D. Geochemical Controls on Lead Concentrations in Stream Water and Sediments. *Geochim. Cosmochim. Acta,* **1976**, *40* (6), 599-609.

7. Martell, A. E.; Smith, R. M.; Motekaitis, R. *NIST Critical Stability Constants of Metal Complexes Database 46;* National Institute of Standards and Technology, Gaithersburg, MD, **2001**.
8. *Stumm,* W.; *Morgan,* J. J. *Aquatic Chemistry: An Introduction Emphasizing Chemical Equilibria in Natural Waters*; Wiley-Interscience, New York, **1970**, p. 276.
9. Perrin, D. D.; Dempsey, B. *Buffers for pH and Metal Ion Control,* Chapman and Hall, London, **1974**, 77-103. https://doi.org/10.1002/ange.19750870621
10. Wanninen, E. V.; Ingman, F. Metal Buffers in Chemical Analysis: Part I-Theoretical Considerations. *Pure & Appl. Chem.,* **1987**, *59*, 1681-1692. https://old.iupac.org/publications/pac/1987/pdf/5912x1681.pdf
11. Wanninen, E. V.; Ingman, F. Metal Buffers in Chemical Analysis: Part II-Theoretical Considerations. *Pure & Appl. Chem.,* **1991**, *63* (4), 639-642. https://old.iupac.org/publications/pac/1991/pdf/6304x0639.pdf
12. Hossain, M.M.; Modelling of Aqueous Equilibrium: Three-Dimensional Trend Surfaces (Topos). Ph. D. Dissertation, University of Montana, Missoula, MT. 2015. https://scholarworks.umt.edu/etd/4413